Research article

Functional division of the dorsal striatum based on a graph neural network

Qian Zheng[1], Xiaojuan Ba[1], Yiyang Xin[3], Jiaofen Nan[1,*], Xiao Cui[1], Lin Xu[2,*]

[1] College of Software Engineering, Zhengzhou University of Light Industry, Zhengzhou 450000, China
[2] College of Intelligent Medicine, Chengdu University of Traditional Chinese Medicine, Chengdu 611137, China
[3] School of Clinical Medicine, Henan University, Zhengzhou 450000, China

* **Correspondence:** Email: nanjiaofen@163.com, xulin@cdutcm.edu.cn; Tel: +8615803898771, +8618780206202.

Abstract: The dorsal striatum, an essential nucleus in subcortical areas, has a crucial role in controlling a variety of complex cognitive behaviors; however, few studies have been conducted in recent years to explore the functional subregions of the dorsal striatum that are significantly activated when performing multiple tasks. To explore the differences and connections between the functional subregions of the dorsal striatum that are significantly activated when performing different tasks, we propose a framework for functional division of the dorsal striatum based on a graph neural network model. First, time series information for each voxel in the dorsal striatum is extracted from acquired functional magnetic resonance imaging data and used to calculate the connection strength between voxels. Then, a graph is constructed using the voxels as nodes and the connection strengths between voxels as edges. Finally, the graph data are analyzed using the graph neural network model to functionally divide the dorsal striatum. The framework was used to divide functional subregions related to the four tasks including olfactory reward, "0-back" working memory, emotional picture stimulation, and capital investment decision-making. The results were further subjected to conjunction analysis to obtain 15 functional subregions in the dorsal striatum. The 15 different functional subregions divided based on the graph neural network model indicate that there is functional differentiation in the dorsal striatum when the brain performs different cognitive tasks. The spatial localization of the functional subregions contributes to a clear understanding of the differences and connections between functional subregions.

1. Introduction

The dorsal striatum, which is composed of the caudate nucleus and putamen, is the entrance to the basal ganglia and receives convergent excitatory afferents from the cortex and thalamus. It forms the origin of direct and indirect pathways and various basal ganglia circuits involved in motor control, mostly for tasks such as action initiation, timing, controlling, learning, and memory [1]. For example, the release of dopamine in the dorsal striatum increases when humans are provided with the opportunity to receive monetary rewards or even stimulated by food in a state of hunger. The brain reacts in a similar way when processing negative emotions and accessing "N-back" working memory [2–4]. Blood oxygen level dependence (BOLD) in the dorsal striatum is increased when the brain is stimulated with choice or decision-related aspects of expected reward value [5]. Based on several types of research, it is generally accepted that the caudate in the dorsal striatum contributes to cognitive functions, while the putamen is mainly involved in motor functions but to some extent also in cognitive functions [6]. Many pathophysiological models of psychiatric disorders (including Huntington's disease, Parkinson's disease, and Alzheimer's disease) include key roles for the caudate and the putamen, as they are closely linked to other regions known to be involved in dysfunction in psychiatric conditions [7–9]. Therefore, it is particularly important to functionally locate the different subregions in the dorsal striatum and to explore the connections between them.

The combination of deep learning algorithms and medical imaging has led to advances in research on the relationship between brain structure and brain function. Traditional deep learning has demonstrated powerful capabilities in medical image anomaly detection, anatomical structure detection and segmentation, and computer-aided diagnosis [10]. However, conventional formulations are limited to data structured in an ordered grid-like fashion, whereas the structure of brain images has a spherical topology (i.e., cortical or subcortical regions); traditional deep learning models have limited ability to capture information about complex curved neighborhoods. With the in-depth research in the field of brain science based on graph theory analysis, models such as Generative Adversarial Networks (GAN) [11–13] and Graph Neural Networks (GNN) [14,15] are widely used in brain functional connectivity, functional magnetic resonance imaging (fMRI) classification, and disease prediction and so on. Moreover, GNN can learn features in a large number of complex and irregular topologies in the cortex or subcortical regions, showing powerful generalization ability and interpretability.

In 2005, Gori et al. [16]. proposed the first GNN, which was a paradigm for machine learning through relationships between data samples. The use of GNN to analyze graph-structured data has received a lot of attention in recent years, leading to considerable progress. In 2022, Campbell et al. [17] proposed the dynamic brain graph structure learning (DBGSL) framework, which showed powerful capabilities in gender classification based on fMRI data. In the same year, Kan et al. [18] proposed the functional brain network generation (FBNETGEN) network to perceive and interpret fMRI data through tasks generated by deep brain networks; the method was applied to two fMRI datasets to validate its effectiveness. Recently, Zheng et al. [19] proposed the Granger causality-inspired GNN (CI-GNN) to diagnose brain disease datasets using functional connectivity within brain regions. The outstanding

results obtained by constructing brain networks and performing functional connectivity analysis in the irregular spherical topology of the brain based on graph theory provide an important idea for the study of the dorsal striatum in this paper. A study of the existing literature reveals that there are fewer related works on the detailed division of the functions of the dorsal striatum and most of the attention has been focused on a single function. In order to fill in the gaps in the study of the functions of the dorsal striatum brain regions, we propose to utilize a graph neural network to carry out the functional division of the dorsal striatum.

In this paper, we propose a framework for functional division of the dorsal striatum based on BrainGNN model, which is further improved on the BrainGNN model proposed by Li et al. [20]. Different from previous graph neural network analysis, instead of using brain regions as network nodes, we constructed brain networks in the dorsal striatum using voxels as nodes, and analyzed the brain networks in the dorsal striatum using the BrainGNN model to filter out subregions with strong correlation with the corresponding functions. To our knowledge, this is the first work to consider the dorsal striatum as the region of interest (ROI), the framework for functional division of the dorsal striatum based on BrainGNN model involves several steps of data preprocessing, extraction of the time series of voxels from the dorsal striatum, and calculation of functional connectivity and functional division by BrainGNN. The division principle is as follows: nodes and edges jointly constructed the graph, so to construct the graph data in the dorsal striatum, nodes and edges features have to be determined first. All voxels in the dorsal striatum are extracted and modeled as nodes, the Pearson correlation coefficient matrix between the nodes is calculated as the different embedding of the node features, and the partial correlation coefficient matrix between the nodes is used as the edge weights of the node connections. Finally, using the BrainGNN model to analyzed the graph data in the dorsal striatum and obtain four functional subregions, namely, olfactory reward, "0-back" working memory, emotional picture stimulation, and capital investment decision-making, the purpose of functional division of the dorsal striatum is achieved.

2. Materials and methods

2.1. Data acquisition

Four mutually independent fMRI datasets for reward, emotion, memory, and decision-making tasks were used. All data were obtained from the publicly available database OpenNeuro. All subjects for the reward-type task were recruited by the University of Geneva; two subjects' fMRI data were excluded for special reasons during the acquisition. In the reward task, twelve olfactory stimuli were administered to 22 subjects, with chocolate olfactory stimuli used as the olfactory reward, and fMRI data were obtained for all subjects. For the emotion-type task, 34 subjects were recruited by Columbia University, and finally 32 subjects' fMRI data were acquired by administering neutral versus aversive picture stimuli to participants. Data on "0-back" working memory were recruited from the Center for Neurosciences in Psychiatric Disorders (CCNMD) at the University of Washington, where 99 subjects (41 healthy controls, 58 people with schizophrenia) performed the "0-back" working memory task, excluding one healthy subject. fMRI data of 40 healthy subjects who performed the "0-back" task were selected for the experiment. The decision-making task involved 20 subjects, who made a choice between making a financial commitment or not. Healthy subjects were selected for all four datasets. Table 1 summarizes the statistics for the four datasets.

Table 1. fMRI data information.

fMRI data	Subject	Age	Men/women	Data acquisition	Data download
Olfactory reward task [21]	22	18–35	13/11	TR = 2400 ms, TE = 41 ms, flip angle = 75°	https://openneuro.org/datasets/ds003487/
Emotional picture stimulation task [22]	32	18–41	15/17	TR = 2000 ms, TE = 40 ms, flip angle = 60°	https://openneuro.org/datasets/ds000108/
"0-back" working memory task [23]	40	12–28	23/17	TR = 2500 ms, TE = 27 ms, flip angle = 90°	https://openneuro.org/datasets/ds000115/
Capital investment decision-making task [24]	20	20–55	5/15	TR = 1900 ms, TE = 2.52 ms, flip angle = 90°	https://openneuro.org/datasets/ds001882/

2.2. The proposed method

Owing to the ability of GNNs to learn features in a large number of complex and irregular topologies, and their powerful generalization ability and interpretability, in this paper, we propose a framework for functional division of the dorsal striatum using the BrainGNN model. The flowchart of the proposed framework is shown in Figure 1.
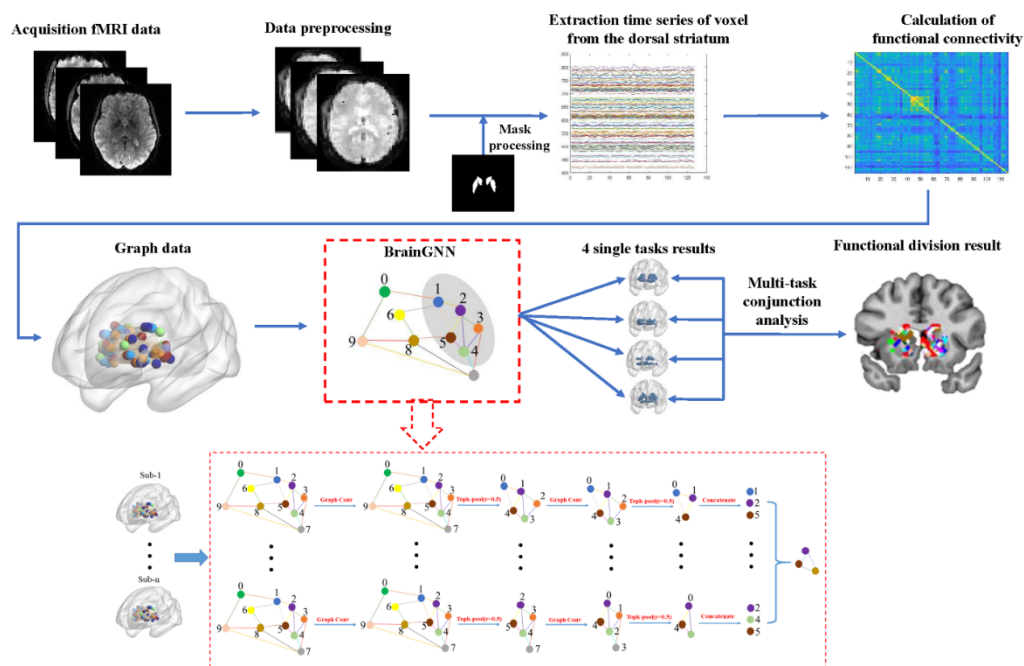
Figure 1. Functional division flowchart in the dorsal striatum based on BrainGNN.

2.2.1. Data preprocessing

Among the non-invasive or minimally invasive techniques suitable for human brain research, fMRI is unmatched to date in terms of its spatiotemporal coverage and information content as a technique for

investigating neuronal activity and brain functional connectivity [25]. However, fMRI data may contain artifacts due to slight movements of the body and spontaneous fluctuations of neurons or the brain during the acquisition process, or due to some other source of noise or signals causing disturbance. Preprocessing of fMRI data in this experiment was performed using the DPABI toolbox [26], with steps including: (1) Removing the first 10 time points of brain images for each subject's data; (2) performing layer time correction and head motion correction for each slice of every brain image; (3) aligning each subject's functional images to their structural images to obtain high-resolution functional images; (4) normalizing all images to the MNI (Montreal Neurological Institute) [27] space at $3 \times 3 \times 3mm^3$ resolution; (5) spatial smoothing using a 4-mm full width at half maximum Gaussian kernel; (6) removal of linear drift; and (7) filtering using a 0.01–0.1 Hz bandpass filter.

2.2.2. Extraction of time series of voxels from dorsal striatum

After preprocessing with the DPABI toolbox, the fMRI data were four-dimensional (4D). A 4D fMRI image is a series of three-dimensional (3D) brain models, which are themselves sequences of two-dimensional brain image slices; the fourth dimension is time. Here, the 4D data were converted into a form that can be read by the GNN. Subjects' 4D data were first converted into T 3D images (where T is the time point of interest) using the dcm2niigui software package. A mask of the dorsal striatum was also drawn using the Anatomical Automatic Labeling (AAL) atlas [28]. Then, the numbers of voxels in the brain regions of the dorsal striatum were extracted from all subjects' 3D images using this mask and used as the number of nodes in the constructed graph. Finally, using the 4D image, the time series of each voxel in the dorsal striatum of each subject was calculated with a size of T × N (where N is the number of nodes). The flowchart of the process of extracting the time series of voxels from the dorsal striatum using the fMRI data of one subject is shown in Figure 2.
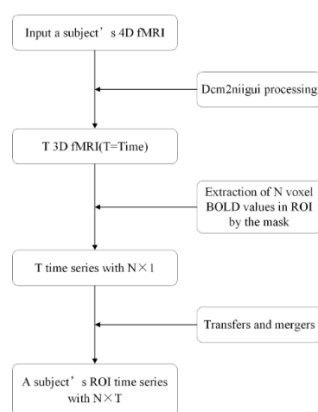

Figure 2. The flowchart of extracting the time series of voxels from the dorsal striatum.

2.2.3. Calculation of functional connectivity

The Pearson correlation coefficient matrix and the partial correlation matrix were computed as node features and edge features, respectively, from the time series of all voxels extracted from each subject's dorsal striatal brain region species. This was because Pearson correlation and partial correlation are different measures of fMRI connectivity. All nodes were aggregated by constructing

edge connections as well as node features, based on recent work on multigraph fusion for neuroimaging analysis [29,30].

The Pearson correlation coefficient matrix was calculated as follows:

$$\rho_{xy} = \frac{\sum_{i=1}^{n}(x_i - \bar{x})(y_i - \bar{y})}{\sqrt{\sum_{i=1}^{n}(x_i - \bar{x})^2 \sum_{i=1}^{n}(y_i - \bar{y})^2}} \tag{1}$$

The Pearson correlation coefficient matrix had $N \times N$ dimensions, and the correlation coefficient values ranged from −1 to 1. When the correlation coefficient value for variables x and y is close to 0, the two variables have low correlation; if the value is positive, the two variables are positively correlated, otherwise, they are negatively correlated.

The partial correlation matrix was calculated by excluding the effects of other variables when calculating the correlation between two variables. For the variable matrix X, the partial correlation coefficient matrix was calculated as follows:

$$\rho_{ij} = \frac{k_{ij}}{\sqrt{k_{ii}k_{jj}}} \tag{2}$$

where $k = (Cov(X))^{-1}$. The partial correlation matrix was also an $N \times N$-dimensional matrix with values in the range $[-1,1]$.

2.2.4. Functional division by BrainGNN

The node and edge features obtained using the method described above were used as inputs to the BrainGNN. The node features were embedded into the low-dimensional space, and the node and edge features were merged to aggregate and update the node vectors. Finally, a pooling operation was performed to output powerfully connected nodes, which were aggregated to form the significance cluster. The specific steps for feature partitioning using this model are as follows.

Step 1: Graph construction. In this work, we use a dorsal striatum mask to divide the subject's fMRI data into N voxels, which are defined as N nodes in the graph $v = (v_1, v_2, ..., v_n)$ (v_i is the i-th node in the graph). Then, we define an undirected weighted graph $G = (v, \varepsilon)$, where ε is the edge set, i.e., (v_i, v_j), a collection of links from v_i to v_j. The matrix $H = [h_1, h_2, ..., h_N]^T$ represents the set of features with associated nodes, and the matrix H is calculated by Pearson correlation function as the node features. h_i is the feature vector associated with node v_i. For each edge between two connected nodes, $(v_i, v_j) \in \varepsilon$, we define $e_{ij} \in \mathbb{R}$ and also $e_{ij} = 0 \notin \varepsilon$, so that there is an adjacency matrix $E = [e_{ij}] \in \mathbb{R}^{N \times N}$, and the matrix E is calculated by the partial correlation function as the edge features. Based on the above analysis, matrix H and matrix E jointly construct the graph data.

Step 2: Graph convolutional layer. The graph convolution layer in the BrainGNN model uses different weights to learn each node embedding. The connection strength between two voxels, i.e., the edge weight, is used for message filtering, because the edge features contain essential information about the graph. In the convolution layer, $h_i^{(l)} \in \mathbb{R}^{d^{(l)}}$ is defined as the feature of the i-th node at the l-th layer, and $d^{(l)}$ is the dimension of the l-th layer feature. The propagation model for node update is:

$$\tilde{h}_i^{(l+1)} = relu(W_i^{(l)}h_i^{(l)} + \sum_{j\in P^{(l)}(i)} e_{ij}^{(l)}W_j^{(l)}h_j^{(l)}) \tag{3}$$

where $P^{(l)}(i)$ denotes the set of indices of neighboring nodes of node v_i, $e_{ij}^{(l)}$ denotes the features associated with the edge from v_i to v_j, and $W_i^{(l)}$ denotes the model's parameters to be learned. As the first layer operates on the original graph, $h_i^{(0)} = h_i$ and $e_{ij}^{(0)} = e_{ij}$. To avoid increasing the scale of output features, the edge features are normalized:

$$e_{ij}^{(l)} = \frac{e_{ij}^{(l)}}{\sum_{j\in P^{(l)}(i)} e_{ij}^{(l)}} \tag{4}$$

The convolutional layer also takes into account the position information of the nodes, which represented not by the coordinates of the nodes but using one-hot encoding. For node v_i, we define its position information γ_i, which is a N-dimensional vector with i-th value 1 and the other values 0. Then, the vectorized embedding kernel $vec(W_i^{(l)})$ of the convolutional layer at the l-th layer based on γ_i is:

$$vec(W_i^{(l)}) = \theta_2^{(l)}relu(\theta_1^{(l)}\gamma_i) + b^{(l)} \tag{5}$$

where parameters $(\theta_1^{(l)}, \theta_2^{(l)})$ map γ_i to a $d^{(l+1)}, d^{(l)}$-dimensional vector, which reshapes the output to a $d^{(l+1)} \times d^{(l)}$ matrix $W_i^{(l)}$. Here, $b^{(l)}$ is the bias term.

Step 3: Graph pooling layer. To keep the indicative nodes in the dorsal striatum, the Topk pooling method proposed by Cannea et al. [31] and Gao and Ji [32] is used to reduce the number of nodes in the graph. In this layer, the node features are projected to the learnable vector $\Gamma^{(l)} \in \mathbb{R}^{d^{(l)}}$ to determine the nodes to be discarded; the nodes with lower scores experience less feature retention. Thus, the $l+1$-th node feature matrix is denoted by $\tilde{H}^{(l+1)} = [\tilde{h}_1^{(l+1)},...,\tilde{h}_{N^{(l)}}^{(l+1)}]^T$, and the Topk pooling layer operation is represented as follows:

$$\begin{aligned}
s^{(l)} &= \tilde{H}^{(l+1)}\Gamma^{(l)}/\|\Gamma^{(l)}\|_2 \\
\tilde{s}^{(l)} &= (s^{(l)} - \mu(s^{(l)}))/\sigma(s^{(l)}) \\
i &= topk(\tilde{s}^{(l)}, k) \\
H^{(l+1)} &= (\tilde{H}^{(l+1)} \odot sigmoid(\tilde{s}^{(l)}))_{i,:} \\
E^{(l+1)} &= E_{i,i}^{(l)}.
\end{aligned} \tag{6}$$

where $\|\cdot\|$ is the second norm, and μ and σ take the input vector and output the mean and standard deviation of its elements. The Topk pooling method finds the index corresponding to the largest k elements of the scoring vector $\tilde{s}$, $\odot$ is element-wise multiplication, and $(\cdot)_{i,j}$ is an indexing operation which takes elements at row indices specified by i and column indices specified by j. The colon in the equation indicates all indices. The pooling operation retains sparsity by requiring only a projection, a point-wise multiplication, and a slicing into the original feature and adjacency matrix.

The BrainGNN model rationalizes the selection of nodes in the graph pooling layer by using Topk pooling (TPK) loss. That is, the first selected node in the graph pooling layer is expected to have a significantly different score compared with the unselected node. Ideally, the scores of selected nodes will be close to 1, whereas those of unselected nodes will be close to 0. Then, the node scores of the m-th input number of M samples are sorted in descending order and denoted by $\hat{s}_m^{(l)} = [\hat{s}_{m,i}^{(l)}, ..., \hat{s}_{m,N^{(l)}}^{(l)}]$. In the BrainGNN model, the TPK loss is expressed as:

$$L_{TPK}^{(l)} = -\frac{1}{M}\sum_{m=1}^{M}\frac{1}{N^{(l)}}(\sum_{i=1}^{k}\log(\hat{s}_{m,i}^{(l)}) + \sum_{i=1}^{N^{(l)}-k}\log(1-\hat{s}_{m,i+k}^{(l)})) \tag{7}$$

Step 4: Node output. To summarize the output graph of the l-th conv-pool block, we perform a flattening operation to retain information about the input graph at a fixed size, using the following equation:

$$z^{(l)} = \text{mean } H^{(l)} \,\|\, \max H^{(l)} \tag{8}$$

where $H^{(l)} = [h_i^{(l)} : i = 1, ...N^{(l)}]$, $\|$ denotes concatenation. To retain useful information in the graph, we concatenate both mean and maximum summarization for a more informative representation.

Step 5: Node clustering. According to the graph input location information, the node location information output from layer l is counted with the pooling score. In the Topk pooling layer, the first k nodes retained after one pooling are reconstructed as an undirected weighted subgraph. The node indexes are also restarted from 0, and then the next convolution and pooling operation is performed. Thus, for any dataset, the node index of the l-th layer output of each subject can be used to find its corresponding $l-1$-th layer node index, and so on, to find the initial node index corresponding to the node output of the l-th layer. This step is repeated to count all output node information of several subjects in a dataset. Then, these nodes are counted, and the nodes with most repetitions are aggregated in combination with the index information of all voxels in the mask. Finally, the aggregated clusters are mapped to the standard brain atlas. The converged clusters are indexed by the nodes (i.e., voxels) of the aggregated output of the pooling layer and can be used to explain the salience of brain activation under a given task.
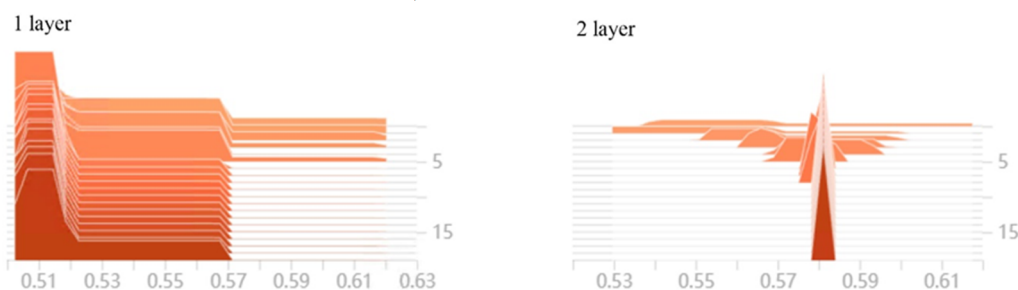
3. Results

3.1. Experimental parameters

The experiment was conducted using the data and method presented in sections 2. After the data had been preprocessed, a total of 1189 voxels were extracted from the dorsal striatum of the fMRI data of each subject, so the node features were $h_i^{(0)} \in \mathbb{R}^{1189}$. Then, based on the functional connectivity between voxels, an undirected weighted graph for the dorsal striatum of each subject was defined, with 1189 nodes per subject in each task condition; 22, 32, 40, and 20 graphs were acquired for the four fMRI datasets, respectively. We ran the algorithm on a Windows 10 operating system with Pytorch in the Python environment using a NVIDIA GeForce GTX 3080Ti with 12GB memory. To determine the pooling rate and the number of convolutional layers to be used in the model, the best pooling rate and the best number of convolutional layers was selected from $\{0.1, 0.2, 0.3, 0.4, 0.5, 0.6, 0.7, 0.8, 0.9, 1.0\}$ and $[1,2]$ for the dataset used in this experiment. The experimental results are shown in Figure 3. Figure 3(A)

shows the differences between the maximum and minimum values of node scores after the one-layer convolution and pooling operations; the smaller the difference, the more converged the selected node scores. As shown in the figure, the best pooling rate of 0.5 was selected. Experiments were conducted on the number of convolution layers with the 0.5 pooling rate, and two-layer convolution with the pooling operation was found to be more selective with indicative nodes. The results are shown in Figure 3(B). After the above experiments, the model consisted of two convolutional and pooling layers with final experimental parameters: $d^{(0)} = 1189$, $d^{(1)} = 32$, $d^{(2)} = 32$, and a pooling rate of 0.5. 596 nodes were retained after 1-th convolutional pooling and 298 nodes were retained after 2-th convolutional pooling with these optimal parameters, the node codes output by each subject under each functional task were counted and sorted, and the top 298 nodes in terms of repetition rate were selected for aggregation as the significantly activated subregions under that functional task.
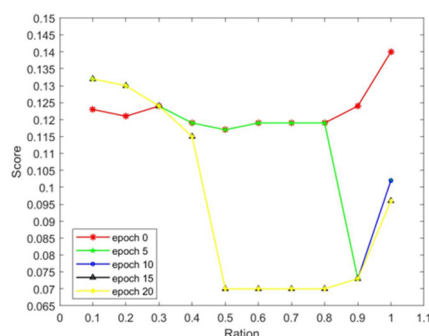
(A) Maximum and minimum difference of node scores after 1 layer convolution and pooling operation. (Horizontal axle: pooling ration; vertical axle: maximum and minimum difference of node scores.)

(B) Node scores for different convolution layers. (Horizontal axle: node scores; vertical axle: epoch.)

Figure 3. Experimental results with different pooling rates and number of convolution layers.

3.2. Single-task results

After analyzing the four task datasets by the method described above, the initial index values corresponding to the 298 voxels in the dorsal striatum under each task were obtained with their corresponding mean scores. These 298 voxels converged into cluster sub-functional areas belonging to each task. Convergence results were mapped to the Ch2 brain atlas and then viewed and analyzed using Mango software (https://mangoviewer.com/mango.html). The functional subregion associated with olfactory reward was defined as ordinate 1, where the central coordinates are located in MNI space (−1,13, 8). This subregion was mainly concentrated in the right caudate body; fewer voxels were

aggregated in the putamen. The functional subregion associated with the "0-back" working memory task, defined as ordinal number 2, was centered in MNI space (1,12.5,7); more voxels were found to converge in the caudate and putamen on the left side of the brain, with relatively few on the right side. The clusters obtained under different emotional picture stimuli were defined as functional subregion 3. This subregion had more activation of voxels in the caudate versus the putamen, with significantly more left than right in the putamen, and its center was located in the MNI space of (1,8,9). Finally, the functional subregion associated with the capital investment decision-making task was defined as ordinate 4, where the central coordinate was located in MNI space (5.5,9,7); this subregion was mainly concentrated in the left caudate body and putamen, with fewer voxels found in the caudate head and the right putamen. Table 2 shows the minimum and maximum values of voxel scores and the percentages of voxel numbers in the dorsal striatum for the four functional subregions. The results of the four functional subregions are shown in Figure 4.

Table 2. Minimum and maximum values of voxel scores and percentages of voxel numbers in the dorsal striatum for the four functional subregions.

Functional subregion No.	Minimum	Maximum	Left		Right	
			Caudate	Putamen	Caudate	Putamen
1	0.5698	0.6015	9.17%	2.76%	11.68%	1.38%
2	0.5824	0.6005	10.20%	3.70%	8.55%	2.54%
3	0.5927	0.6030	8.08%	5.83%	8.08%	3.01%
4	0.6006	0.6078	7.39%	8.87%	5.67%	3.08%

Functional subregion No. = Functional subregion number; Minimum = the node minimum score; Maximum = the node maximum score; Percentage = the voxel numbers of functional subregion No. in left caudate or left putamen or right caudate or putamen/1189.
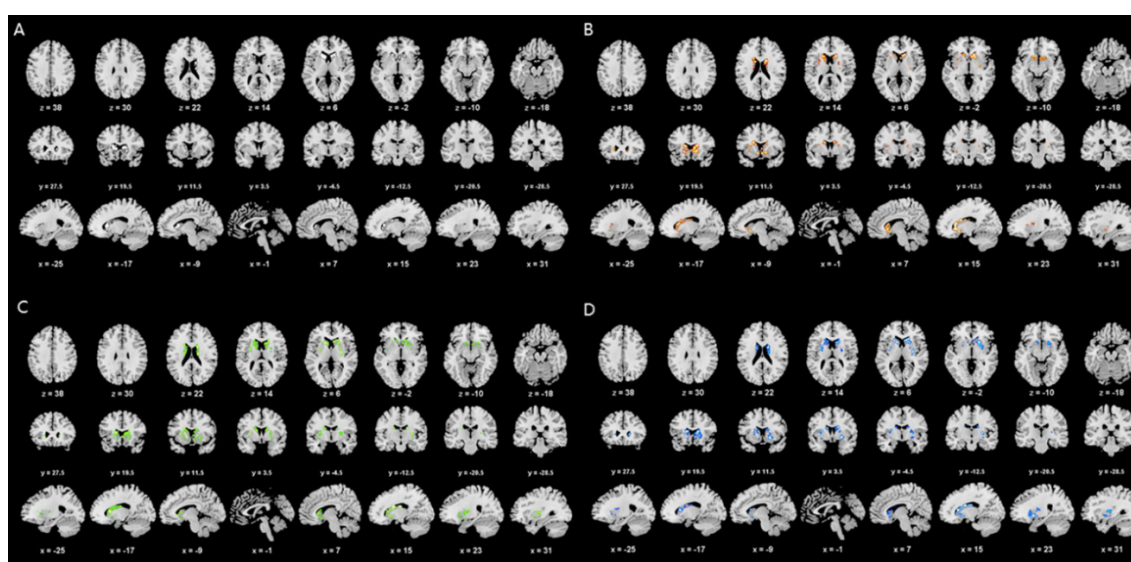

Figure 4. The results of 1–4 functional subregions. (A) 1: the result of olfactory reward task; (B) 2: the result of "0-back" working memory task; (C) 3: the result of emotional picture stimulation task; (D) 4: the result of capital investment decision-making task.

3.3. Multi-task conjunction results

In this work, four single tasks were used to divide the dorsal striatum into four different functional subregions. Then, the results of the individual tasks were used to analyze the differences and connections between these regions to explore the functional subregions of the caudate and putamen under the influence of multiple tasks. The conjunction of any two tasks was displayed and analyzed using Mango software as well as the Ch2 brain atlas. The olfactory reward task was combined with the "0-back" working memory task, emotional picture stimulation task, and capital investment decision-making task. The functional subregions showing combined activation were defined as ordinal numbers 5, 6, and 7, which were located in MNI space (−2,15,8), (0,11.5,11), and (3,11.5,9.5), respectively. Functional subregion 5 was more activated in the caudate head than in the caudate body. However, functional subregions 6 and 7 showed the opposite pattern of activation. The "0-back" working memory task was jointly analyzed with the emotional picture stimulation task and the capital investment decision-making task, respectively. Their joint functional subregions were defined as numbers 8 and 9, with central coordinates located in MNI space (1.5,13,9) and (4.5,13.5,9). Similarly, functional subregion 8 was more concentrated in the caudate body in the left caudate, and the right side was concentrated in the caudate head. Functional subregion 9 was activated far more significantly on the left side than the right side and was more concentrated in the caudate body and the tail of the putamen. Last, the conjunct outcome of the emotional picture stimulation task and the capital investment decision-making task was defined as functional subregion 10, which was centered at coordinates in MNI space (4.5,9,9). In this case, the left side of the brain was more concentrated in the caudate body, and significant activation in the right side of the putamen was observed in all putamen subregions except for the head of the putamen, where no significant activation was found. Table 3 shows the percentages of the numbers of voxels in the dorsal striatum in functional subregions 5–10. The conjunction results of functional subregions 5–10 are shown in Figure 5.

Table 3. Percentages of numbers of voxels in the dorsal striatum in functional subregions 5–10.

Functional subregion No.	Left		Right	
	Caudate	Putamen	Caudate	Putamen
5	3.53%	0.58%	3.92%	0.34%
6	2.90%	1.27%	3.24%	0.33%
7	4.71%	1.96%	3.73%	0.74%
8	2.07%	0.50%	1.80%	0.22%
9	2.82%	1.26%	1.90%	0.48%
10	2.73%	2.43%	2.60%	0.64%

Functional subregion No. = Functional subregion number; Percentage = the voxel numbers of functional subregion No. in left caudate or left putamen or right caudate or putamen/1189.

As described above, we performed conjunction analyses with each of the three tasks. The functional subregion that defined the joint activation of the olfactory reward task, the "0-back" working memory task, and the emotional picture stimulation task was denoted by ordinal number 11; the functional subregion for the olfactory reward task, "0-back" working memory task, and capital investment decision-making task was denoted 12; the functional subregion for the olfactory reward

task, emotional picture stimulation task, and capital investment decision-making task was 13, and the "0-back" working memory task. The functional subregion corresponding to joint activation by the emotional picture stimulation task and the capital investment decision-making task was denoted 14. The center coordinates of these four functional areas were located in MNI space (1,11.5,8.5), (3.5,14,9.5), (3,11,10), and (3.5,13.5,9.5), respectively. Significant activation areas for functional subregions 11 and 14 in the left brain were concentrated in the caudate body, whereas those for the right side were in the caudate head, and fewer voxels were found in the left and right putamen. Functional subregions 12 and 13 had more voxels in the left and right caudate than functional subregions 11 and 14, and both were concentrated in the caudate body. Table 4 shows the percentages of the numbers of voxels in the dorsal striatum in functional subregions 11–14. The conjunction results of functional subregions 11–14 are shown in Figure 6.
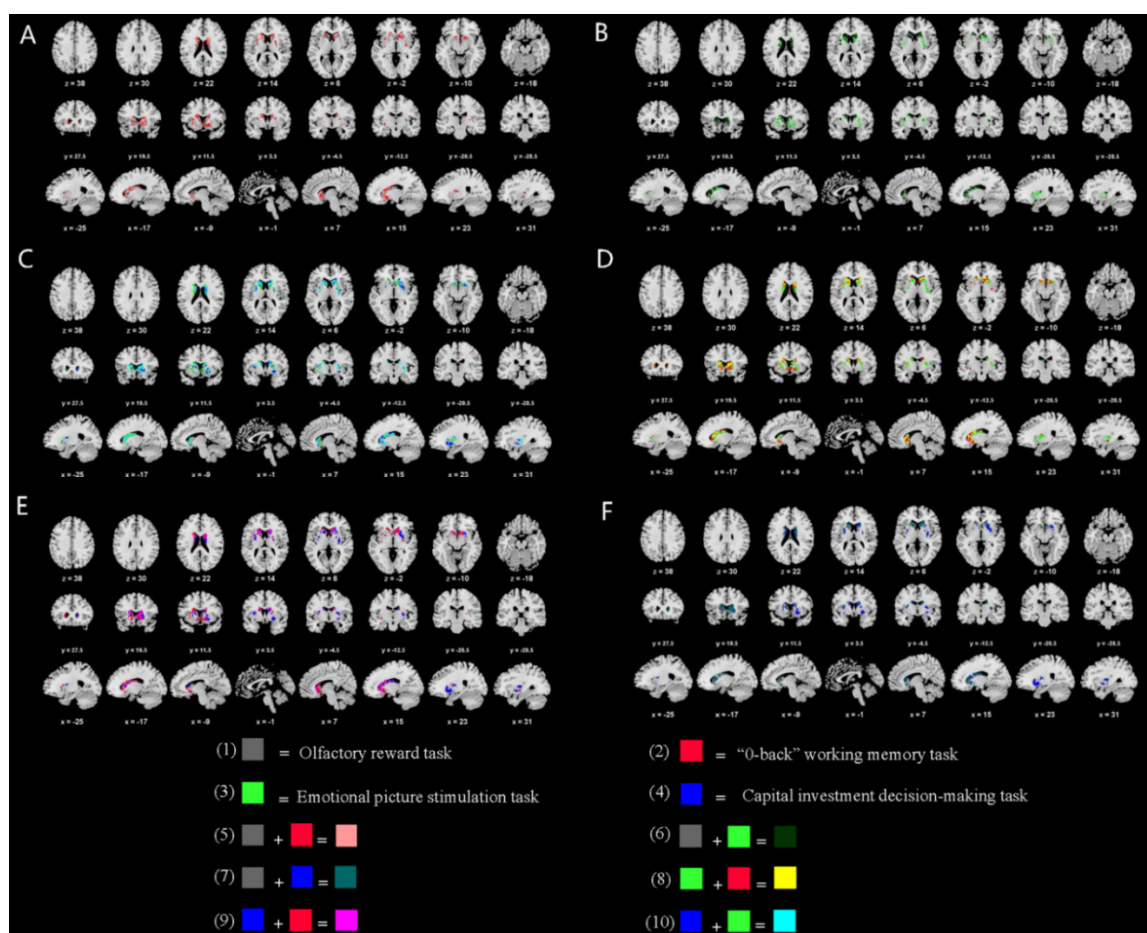

Figure 5. Conjunction results of functional subregions 5–10. (A) 5: The conjunction result of olfactory reward task and "0-back" working memory task; (B) 6: The conjunction result of olfactory reward task and emotional picture stimulation task; (C) 7: The conjunction result of olfactory reward task and capital investment decision-making task; (D) 8: The conjunction result of "0-back" working memory task and emotional picture stimulation task; (E) 9: The conjunction result of "0-back" working memory task and capital investment decision-making task; (F) 10: The conjunction result of emotional picture stimulation task and capital investment decision-making task.

Table 4. Percentages of numbers of voxels in the dorsal striatum in functional subregions 11–14.

Functional subregion No.	Left		Right	
	Caudate	Putamen	Caudate	Putamen
11	1.49%	0.30%	1.59%	0.07%
12	2.28%	0.48%	1.67%	0.21%
13	2.25%	1.27%	2.21%	0.32%
14	1.30%	0.42%	1.17%	0.13%

Functional subregion No. = Functional subregion number; Percentage = the voxel numbers of functional subregion No. in left caudate or left putamen or right caudate or putamen/1189.
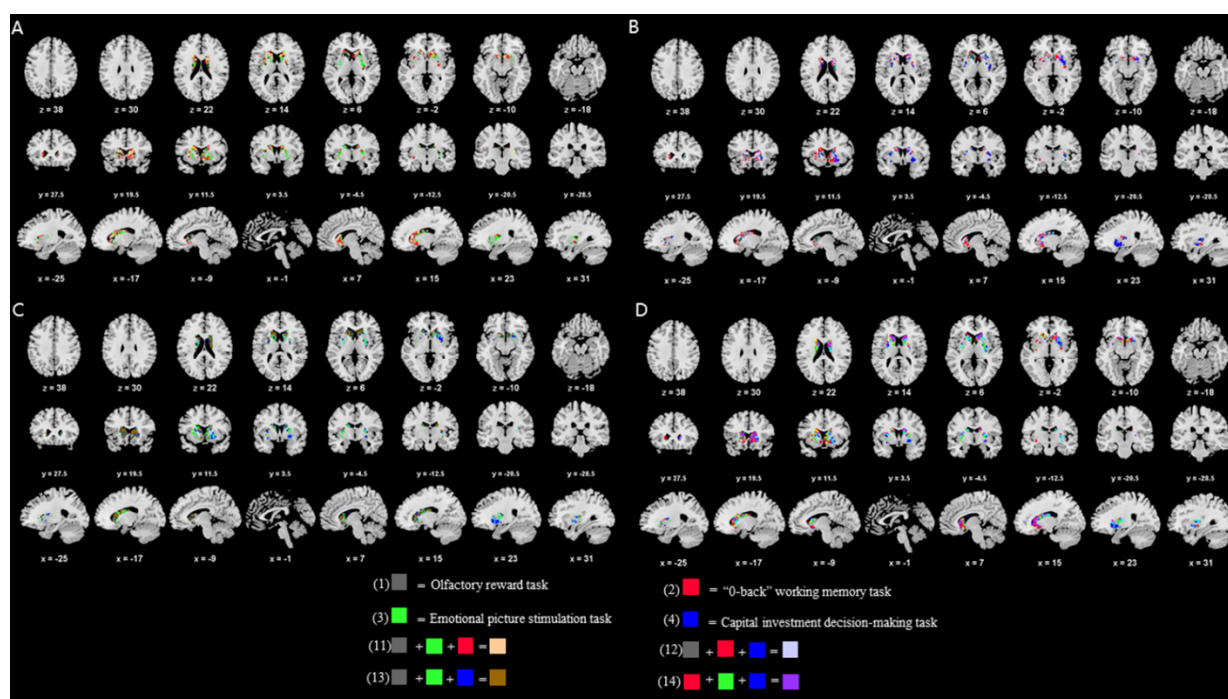

Figure 6. Conjunction results of functional subregions 11–14. (A) 11: The conjunction result of olfactory reward task and "0-back" working memory task and emotional picture stimulation task; (B) 12: The conjunction result of olfactory reward task "0-back" working memory task and capital investment decision-making task; (C) 13: The conjunction result of olfactory reward task and emotional picture stimulation task and capital investment decision-making task; (D) 14: The conjunction result of "0-back" working memory task and emotional picture stimulation task and capital investment decision-making task.

Finally, a conjunction analysis for all four tasks was performed. The functional subregion conjunctly activated by the four tasks was defined by ordinal number 15, and the core coordinate was located in MNI space (2.5,14.5,9.5). Counting the numbers of voxels in functional subregion 15 in the dorsal striatum showed that more voxels were activated in the left caudate than the right, and that they were concentrated in the caudate body, whereas the right putamen was activated by far more voxels than the left. Figure 7 shows the results for co-activation of the dorsal striatum under all four tasks.
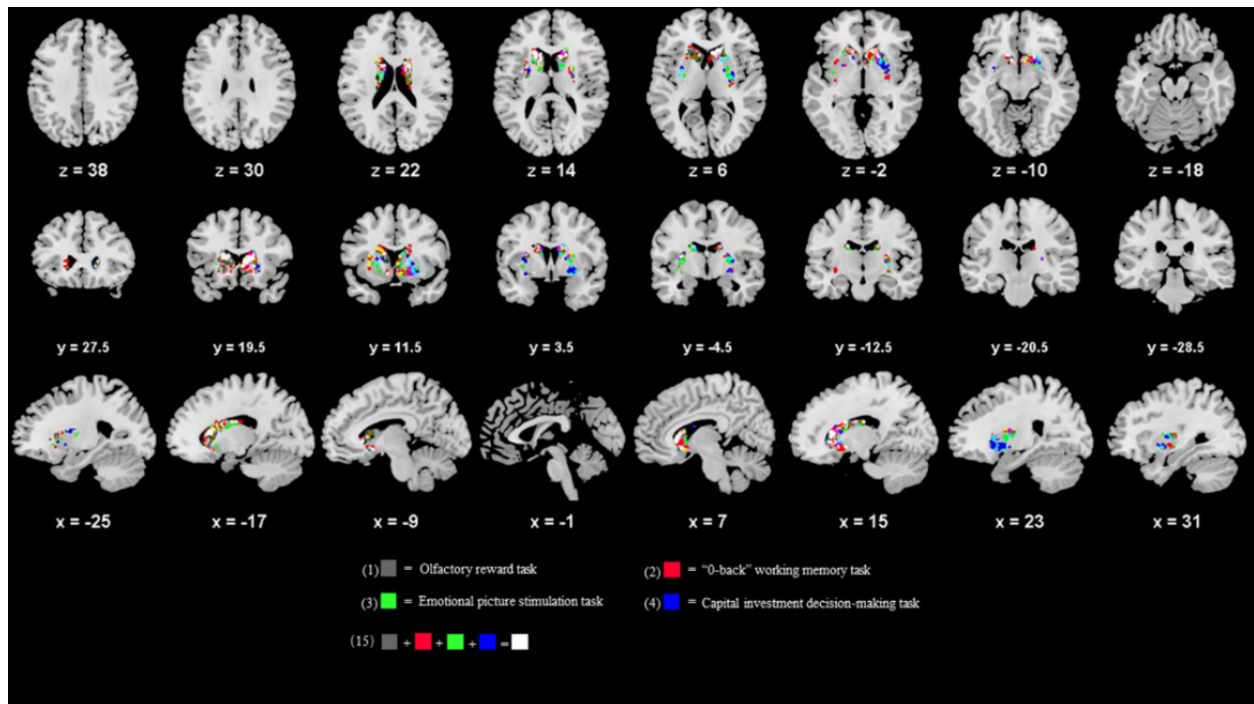
Figure 7. Results of co-activation of the dorsal striatum under four tasks.

3.4. Dorsal striatum functional division results

In this study, a GNN was used to converge the significant activation subregions in the dorsal striatum for olfactory reward, "0-back" working memory, emotional picture stimulation, and capital investment decision-making tasks. The dorsal striatum was then divided into 15 functional subregions, with each functional subregion responsible for different aspects of cognitive control. The 15 functional subregions were labeled with the numbers 1 to 15. The results are shown in Figure 8.

Figure 8. Dorsal striatum functional division results.

4. Discussion

The experimental results obtained using the BrainGNN model indicate that biomarkers of brain regions in response to task stimuli can be characterized by pooling the outputs of nodes with higher repetition rates and thus aggregating them into different clusters. Based on an extensive search of the

literature, we found that most brain studies using GNNs were performed by extracting the average time series of each brain region to calculate the functional connectivity between brain regions. However, in this experiment, the raw fMRI data were first restricted to the caudate and putamen, and the time series of each voxel was obtained by extracting the BOLD values (i.e., voxel values) of each voxel within these two brain regions to calculate the functional connectivity between voxels. Then, each voxel was treated as a node in the graph data, and the Pearson correlation coefficient matrix and partial correlation matrix were calculated using time series of voxels as node features and edge weights, with each node aggregated to neighboring node features by a two-layer convolutional pooling operation. The 1189 voxels extracted from each subject's data were convolved, and each node embedding was obtained after one layer of aggregation. The remaining 595 nodes were pooled again after the pooling operation to obtain the remaining 298 nodes. Finally, the 298 nodes for each subject were counted, and the top 298 nodes with the highest repetitions rate were exported to be aggregated into a cluster.

The fMRI data acquired during four different tasks were studied using the BrainGNN research method in this work. The four different clusters were aggregated in the dorsal striatum, first using single tasks to define functional subregions, and then using conjunction analysis of two, three, or all four tasks. The final division comprised 15 functional subregions. Whereas the left caudate was most activated by the "0-back" working memory task, the right caudate was most activated by the olfactory reward task, and the left and right putamen were the most activated areas for the capital investment decision-making. Based on our analysis, the results for the four tasks showed both connections between and differences in the brain regions activated during different cognitive tasks.

The results described above demonstrate that achieving functional integration is a critical issue. The conjunction analysis of the experimental results from four single tasks revealed multifunctional patterns between different task categories. First, each pair of tasks was conjunctly analyzed, and six different functional subregions were obtained. Among these six functional subregions, the largest clusters were found for the olfactory reward and capital investment decision-making tasks, and these clusters were more concentrated in the left and right caudate body compared with other areas. However, the association of olfactory reward with the "0-back" working memory task was more concentrated in the left caudate head, and the association of picture emotional stimulation with the capital investment decision-making task was more distributed in the putamen. Afterwards, conjunction analysis of each set of three tasks was performed, and the cluster size of each resultant aggregate was counted. The results showed that the joint olfactory reward, emotional picture stimulation, and capital investment decision-making tasks accounted for the largest functional subregions, which were concentrated in the left caudate body and putamen, whereas the left and right caudate head regions were more evenly distributed among the conjunction results for any of the other three tasks. In the final conjunction analysis of all four tasks, more voxels converged in the caudate and putamen in the left side of the brain than in the right side, again concentrated in the caudate body. Using the above experimental process, the dorsal striatum was divided into a total of 15 functional subregions, which are related to different cognitive functions in humans. These findings may be important for future studies of mental disorders involving dysfunction of the caudate and putamen.

The study had some limitations. First, the dorsal striatum masks generated by different brain atlases in the data preprocessing were different, which led to different results in the final division; this has implications for reproducibility and consistency. Second, this study only considered one kind of stimulus for each task, whereas reward stimuli also include money, food, etc. Future studies should

use more comprehensive data for functional division of the dorsal striatum. Finally, the correctness of the division of the dorsal striatum in the future also needs to be verified from many aspects.

5. Conclusions

In this paper, a GNN framework for functional division of the dorsal striatum has been proposed. The framework performs data preprocessing, extraction of voxel time series from the dorsal striatum, calculation of functional connectivity, and BrainGNN model division. Four fMRI datasets were obtained from publicly available databases for an olfactory reward task, "0-back" working memory task, emotional picture stimulation task, and capital investment decision-making task. After the above steps, four subregions of the dorsal striatum were divided into four tasks, and a conjunction analysis was performed through these four functional subregions, resulting in the division of the dorsal striatum into 15 functional subregions. These results will promote a clearer understanding of the differences and connections between functional subregions.

Use of AI tools declaration

The authors declare that they have not used Artificial Intelligence (AI) tools in the creation of this article.

Acknowledgments

Conflict of interest

The authors declare that there are no conflicts of interest.

References

1. D. Riva, M. Taddei, S. Bulgheroni, The neuropsychology of basal ganglia, *Eur. J. Paediatr. Neurol.*, **22** (2018), 321–326. https://doi.org/10.1016/j.ejpn.2018.01.009

2. W. H. Kaye, C. E. Wierenga, A. Bischoff-Grethe, L. A. Berner, A. V. Ely, U. F. Bailer, et al., Neural insensitivity to the effects of hunger in women remitted from anorexia nervosa, *Am. J. Psychiatr. Assoc.*, **177** (2020), 601–610. https://doi.org/10.1176/appi.ajp.2019.19030261

3. M. Yousuf, M. Heldmann, M. Göttlich, T. F. Münte, N. Doñamayor, Neural processing of food and monetary rewards is modulated by metabolic state, *Brain Imaging Behav.*, **12** (2018), 1379–1392. https://doi.org/10.1007/s11682-017-9811-y

4. C. B. Klune, B. Jin, L. A. DeNardo, Linking mPFC circuit maturation to the developmental regulation of emotional memory and cognitive flexibility, *Elife*, **10** (2021), 64567. https://doi.org/10.7554/eLife.64567

5. A. M. Lee, L. Tai, A. Zador, L. Wilbrecht, Between the primate and 'reptilian' brain: Rodent models demonstrate the role of corticostriatal circuits in decision making, *Neuroscience*, **296** (2015), 66–74. https://doi.org/10.1016/j.neuroscience.2014.12.042

6. G. Dong, H. Dong, M. Wang, J. Zhang, W. Zhou, X. Du, et al., Dorsal and ventral striatal functional connectivity shifts play a potential role in internet gaming disorder, *Commun. Biol.*, **4** (2021), 866. https://doi.org/10.1038/s42003-021-02395-5

7. A. Raj, F. Powell, Network model of pathology spread recapitulates neurodegeneration and selective vulnerability in Huntington's disease, *NeuroImage*, **235** (2021), 118008. https://doi.org/10.1016/j.neuroimage.2021.118008

8. X. Liu, S. B. Eickhoff, S. Caspers, J. Wu, S. Genon, F. Hoffstaedter, et al., Functional parcellation of human and macaque striatum reveals human-specific connectivity in the dorsal caudate, *NeuroImage*, **235** (2021) 118006. https://doi.org/10.1016/j.neuroimage.2021.118006

9. K. Simonyan, Recent advances in understanding the role of the basal ganglia, *F1000Research*, **8** (2019), 122. https://doi.org/10.12688/f1000research.16524.1

10. D. Ahmedt-Aristizabal, M. A. Armin, S. Denman, C, Fookes, L, Petersson, Graph-based deep learning for medical diagnosis and Analysis: past, present and future, *Sensors*, **21** (2021), 4758. https://doi.org/10.3390/s21144758

11. C. Gong, C. Jing, X. Chen, C. M. Pun, G. Huang, A. Saha, et al., Generative AI for brain image computing and brain network computing: a review, *Front. Neurosci.*, **17** (2023), 1203104. https://doi.org/10.3389/fnins.2023.1203104

12. J. Pan, B. Lei, Y. Shen, Y. Liu, Z. Feng, S. Wang, Characterization multimodal connectivity of brain network by hypergraph GAN for Alzheimer's disease analysis, preprint, arXiv:2107.09953.

13. Q. Zuo, N. Zhong, Y. Pan, H. Wu, B. Lei, S. Wan, Brain structure-function fusing representation learning using adversarial decomposed-VAE for analyzing MCI, *IEEE Trans. Neural Syst. Rehabil. Eng.*, **31** (2023), 4017–4028. https://doi.org/10.1109/TNSRE.2023.3323432

14. T. N. Kipf, M. Welling, Semi-supervised classification with graph convolutional networks, preprint, arXiv:1609.02907.

15. W. L. Hamilton, R. Ying, J. Leskovec, Inductive representation learning on large graphs, preprint, arXiv:1706.02216.

16. M. Gori, G. Monfardini, F. Scarselli, A new model for learning in graph domains, in *2005 IEEE International Joint Conference on Neural Networks*, **2** (2005), 729–734. https://doi.org/10.1109/IJCNN.2005.1555942

17. A. Campbell, A. G. Zippo, L. Passamonti, N. Toschi, P. Lio, DBGSL: Dynamic brain graph structure learning, preprint, arXiv:2209.13513.

18. X. Kan, H. Cui, J. Lukemire, Y. Guo, C. Yang, Fbnetgen: Task-aware GNN -based fMRI analysis via functional brain network generation, *Proc. Mach. Learn. Res.*, (2022), 618–637.

19. K. Zheng, S. Yu, B. Chen, CI-GNN: A granger Causality-Inspired Graph Neural Network for interpretable brain network-based psychiatric diagnosis, preprint, arXiv:2301.01642.

20. X. Li, Y. Zhou, N. Dvornek, M. Zhang, S. Gao, J. Zhuang, et al., Braingnn: Interpretable brain graph neural network for fMRI analysis, *Med. Image Anal.*, **74** (2021), 102233. https://doi.org/10.1016/j.media.2021.102233

21. E. R. Pool, D. M. Tord, S. Delplanque, Y. Stussi, D. Cereghetti, P. Vuilleumier, et al., Differential contributions of ventral striatum subregions to the motivational and hedonic components of the affective processing of reward, *J. Neurosci.*, **42** (2022), 2716–2728. https://doi.org/10.1523/JNEUROSCI.1124-21.2022

22. T. D. Wager, M. L. Davidson, B. L. Hughes, M, A. Lindquist, K, N. Ochsner, Prefrontal-subcortical pathways mediating successful emotion regulation, *Neuron*, **59** (2008), 1037–1050. https://doi.org/10.1016/j.neuron.2008.09.006

23. G. Repovš, D. M. Barch, Working memory related brain network connectivity in individuals with schizophrenia and their siblings, *Front. Hum. Neurosci.*, **6** (2012), 137. https://doi.org/10.3389/fnhum.2012.00137

24. M. Piva, K. Velnoskey, R. Jia, A. Nair, I. Levy, S. W. Chang, The dorsomedial prefrontal cortex computes task-invariant relative subjective value for self and other, *Elife*, **8** (2019), 44939. https://doi.org/10.7554/eLife.44939

25. K. Uğurbil, Ultrahigh field and ultrahigh resolution fMRI, *Curr. Opin. Biomed. Eng.*, **18** (2021), 100288. https://doi.org/10.1016/j.cobme.2021.100288

26. C. Yan, X. Wang, X. Zuo, Y. Zang, DPABI: data processing & analysis for (resting-state) brain imaging, *Neuroinformatics*, **14** (2016), 339–351. https://doi.org/10.1007/s12021-016-9299-4

27. A. C. Evans, D. L. Collins, S. R. Mills, E. D. Brown, R. L. Kelly, T. M. Peters, 3D statistical neuroanatomical models from 305 MRI volumes, in 1993 IEEE *Conference Record Nuclear Science Symposium and Medical Imaging Conference*, **3** (1993), 1813–1817. https://doi.org/10.1109/NSSMIC.1993.373602

28. A. C. Evans, A. L. Janke, D. L. Collins, S. Baillet, Brain templates and atlases, *Neuroimage*, **62** (2012), 911–922. https://doi.org/10.1016/j.neuroimage.2012.01.024

29. J. Gan, X. Zhu, R. Hu, Y. Zhu, J. Ma, Z. Peng, et al., Multi-graph fusion for functional neuroimaging biomarker detection, in *Twenty-Ninth International Joint Conference on Artificial Intelligence Main track*, (2020), 580–586. https://doi.org/10.24963/ijcai.2020/81

30. X. Yang, Y. Jin, X. Chen, H. Zhang, G. Li, D. Shen, Functional connectivity network fusion with dynamic thresholding for MCI diagnosis, in *International Workshop on Machine Learning in Medical Imaging*, **10019** (2016), 246–253. https://doi.org/10.1007/978-3-319-47157-0_30

31. C. Cangea, P. Veličković, N. Jovanović, T. Kipf, P. Liò, Towards sparse hierarchical graph classifiers, preprint, arXiv:1811.01287.

32. H. Gao, S. Ji, Graph U-Nets, preprint, arXiv:1905.05178.